

# Synthesis of monodisperse silver nanoparticles for ink-jet printed flexible electronics

Zhiliang Zhang<sup>1,2,3</sup>, Xingye Zhang<sup>1,4</sup>, Zhiqing Xin<sup>1</sup>,  
Mengmeng Deng<sup>1</sup>, Yongqiang Wen<sup>1</sup> and Yanlin Song<sup>1,4</sup>

<sup>1</sup> Beijing National Laboratory for Molecular Sciences (BNLMS), Key Lab of Organic Solids, Laboratory of New Materials, Institute of Chemistry, Chinese Academy of Sciences, Beijing 100190, People's Republic of China

<sup>2</sup> Research Center of Analysis and Test, Shandong Polytechnic University, Jinan 250353, People's Republic of China

<sup>3</sup> Graduate University of Chinese Academy of Sciences, Beijing 100049, People's Republic of China

E-mail: [zhangxy@iccas.ac.cn](mailto:zhangxy@iccas.ac.cn) and [ylsong@iccas.ac.cn](mailto:ylsong@iccas.ac.cn)

Received 21 July 2011, in final form 23 August 2011

Published 22 September 2011

Online at [stacks.iop.org/Nano/22/425601](http://stacks.iop.org/Nano/22/425601)

## Abstract

In this study, monodisperse silver nanoparticles were synthesized with a new reduction system consisting of adipoyl hydrazide and dextrose at ambient temperature. By this facile and rapid approach, high concentration monodisperse silver nanoparticles were obtained on a large scale at low protectant/AgNO<sub>3</sub> mass ratio which was highly beneficial to low cost and high conductivity. Based on the synthesized monodisperse silver nanoparticles, conductive inks were prepared with water, ethanol and ethylene glycol as solvents, and were expected to be more environmentally friendly. A series of electrocircuits were fabricated by ink-jet printing silver nanoparticle ink on paper substrate with a commercial printer, and they had low resistivity in the range of  $9.18 \times 10^{-8}$ – $8.76 \times 10^{-8}$   $\Omega$  m after thermal treatment at 160 °C for 30 min, which was about five times that of bulk silver ( $1.586 \times 10^{-8}$   $\Omega$  m). Moreover, a radio frequency identification (RFID) antenna was fabricated by ink-jet printing, and 6 m wireless identification was realized after an Alien higgs-3 chip was mounted on the printed antenna by the flip-chip method. These flexible electrocircuits produced by ink-jet printing would have enormous potential for low cost electrodes and sensor devices.

 Online supplementary data available from [stacks.iop.org/Nano/22/425601/mmedia](http://stacks.iop.org/Nano/22/425601/mmedia)

(Some figures in this article are in colour only in the electronic version)

## 1. Introduction

Ink-jet printing is a particularly attractive alternative to conventional photolithography as a convenient and rapid processing technique to fabricate electrocircuits for direct writing of patterns and the delivery of precise quantities of materials to manufacture electronic devices [1, 2]. This technique is low cost and flexible for mass-production of electrocircuits since it eliminates conventional photolithography and complex substrate processing including vapor phase deposition and

etching [3]. Moreover, ink-jet printing technology can avoid the production of large quantities of chemical waste and is environmentally friendly [4–6]. A major challenge in applying ink-jet processes for depositing materials, among various difficulties and obstacles, is the formulation of suitable inks. Ink chemistry and formulations not only determine the drop ejection characteristics and the compatibility with the print head system, but also dictate the quality of the printed electrocircuits [7]. For metal conductive ink, uniform and monodisperse metal nanoparticles, such as the most commonly used silver nanoparticles, are crucial to attain a stable conductive ink because they contribute to attaining

<sup>4</sup> Authors to whom any correspondence should be addressed.

high dispersion stability and low electrical resistance at low metallization temperature [8].

Up to now, a number of techniques have been developed to synthesize metal nanoparticles [9], such as chemical reduction [10], sonochemical reduction [11], the polyol process [12], radiolytic reduction [13], and solvent-extraction reduction [14]; these are probably the most popular techniques due to their simplicity, low cost and massive scaling-up [15–18]. However, the size distributions of the synthesized nanoparticles with the above approaches are usually wide at high solution concentration. Moreover, it is difficult to obtain monodisperse silver nanoparticles on a large scale at low protectant/precursor mass ratio. The stability of ink based on these synthesized nanoparticles will likely be affected as they aggregate and precipitate out from the solution. More seriously, the nozzle of the printer would be clogged with larger nanoparticles or aggregation, which greatly hinders silver nanoparticle application in ink-jet printed electrocircuits [7].

In order to improve the monodispersity and prevent aggregation of silver nanoparticles, the mass ratio of the protectant/precursors in the synthesis process is usually very high [19], which not only increases the nanofabrication cost but also influences the conductivity of electrocircuits fabricated by ink-jet printing. Although great efforts have been made [16, 17], it remains a great challenge to prepare uniform and monodisperse silver nanoparticles at low protectant/precursors mass ratio in aqueous solution, particularly at high concentration and on a large scale. In this paper, a new reduction system consisting of adipoyl hydrazide and dextrose was used to synthesize silver nanoparticles. Compared with other reductants, such as hydrazine hydrate or sodium borohydride, this reduction system was more environmentally friendly and facile to control. By controlling the nucleation and growth process, monodisperse silver nanoparticles with a high concentration were obtained at ambient temperature, and the reaction system could be conducted on a liter scale. In particular, the mass ratio of protectant/precursors by this approach was very low, which not only reduced the cost but also increased the conductivity of the ink-jet printed electrocircuits. A series of electrocircuits were fabricated by ink-jet printing silver nanoparticle ink on paper with a commercial printer, and they had low resistivity in the range of  $9.18 \times 10^{-8}$ – $8.76 \times 10^{-8} \Omega \text{ m}$  by thermal treatment at  $160^\circ\text{C}$  for 30 min, which was about five times that of bulk silver ( $1.586 \times 10^{-8} \Omega \text{ m}$ ). In order to verify the application performance, an RFID antenna was fabricated by ink-jet printing, and 6 m wireless identification was realized after an Alien higgs-3 chip was mounted on the printed antenna. The flexible electrocircuits by ink-jet printing would have enormous potential for low cost electrodes and sensor devices.

## 2. Experimental details

### 2.1. Materials

Highly concentrated monodisperse silver nanoparticles were prepared from  $\text{AgNO}_3$  (reagent;  $\geq 99\%$ , Aldrich) as silver source materials with adipic dihydrazide (reagent;  $\geq 98\%$ ,

Aldrich) and dextrose (reagent;  $\geq 98\%$ , Sigma) as reducing agent. Polyvinylpyrrolidone (PVP,  $M_w = 1 \times 10^4$ , Aldrich) was used as the protectant to prepare the silver nanoparticles. Anisotropic conductive paste (ACP, BP303) was bought from Sony Chemical Corporation. The RFID chip (Alien higgs-3) came from Alien Technology Co., Ltd. The other chemicals were analytical or high reagent grade.

### 2.2. Preparation of monodisperse silver nanoparticles and conductive ink

Monodisperse silver nanoparticles were prepared by a straightforward, one-phase reaction. In a typical synthesis of silver nanoparticles, 200 ml of 1.5 M aqueous solution of silver nitrate was quickly added into a beaker containing 600 ml of  $6.25 \times 10^{-3}$  M PVP aqueous solution. The mixture was stirred for 10 min to form a Ag–PVP complex at room temperature. Next, the Ag–PVP complex was reduced by addition of 200 ml of freshly prepared aqueous solution of adipoyl hydrazide and dextrose. The products were purified by washing with water, and separated with centrifugation. After drying under vacuum at  $60^\circ\text{C}$  for 30 min, bright-yellow powder was obtained.

To prepare the conductive nanoparticle ink, the synthesized silver nanoparticles were redissolved into the mixture of ethylene glycol, ethanol and water with a mass ratio of about 7:2:1. The silver nanoparticles were dispersed by ball milling to obtain 10–15 wt% silver nanoparticle ink and used for ink-jet flexible printed electrocircuits.

### 2.3. Fabrication of flexible electrocircuits by ink-jet printing

A series of flexible electrocircuits were fabricated by jetting the silver nanoparticle ink onto chrome paper using a commercial Epson C110 printer, and the drop size and drop space were about 3 pl and  $5 \mu\text{m}$  correspondingly. In a typical ink-jet process, an RFID antenna according to the Alien-9662 inlay was obtained with the same ink-jet process. The ink-jet printed samples were sintered in a convection oven at different temperatures, and the sintering time was kept at 30 min. The electrical resistivity,  $\rho$ , was calculated from the resistance  $R$ , the length  $l$ , and the cross-sectional area  $A$  of the line, using  $\rho = RA/l$ , and subsequently compared to the value of bulk silver ( $1.586 \times 10^{-8} \Omega \text{ m}$ ) [20]. The cross-sectional area was determined by numerical integration of the measured profile. Finally, a wireless identification device was obtained after a chip was mounted on the printed RFID antenna by the flip-chip method.

### 2.4. Characterization

Fourier transform infrared spectra in the range of 400–4000  $\text{cm}^{-1}$  were recorded on an FTIR Tensor 27 spectrometer (Bruker, Germany) using KBr pellets. UV spectra of the samples were recorded in a U-4100 (Hitachi, Japan) UV spectrophotometer. X-ray photoelectron spectroscopy (XPS) was recorded on an ESCALab 220i-XL electron spectrometer from VG Scientific using 300 W Al  $K\alpha$  radiation. The base pressure was about  $3 \times 10^{-9}$  mbar. The size and distribution of the synthesized silver nanoparticles were characterized by JEM-2100F transmission electron microscopy (JEOL, Japan)

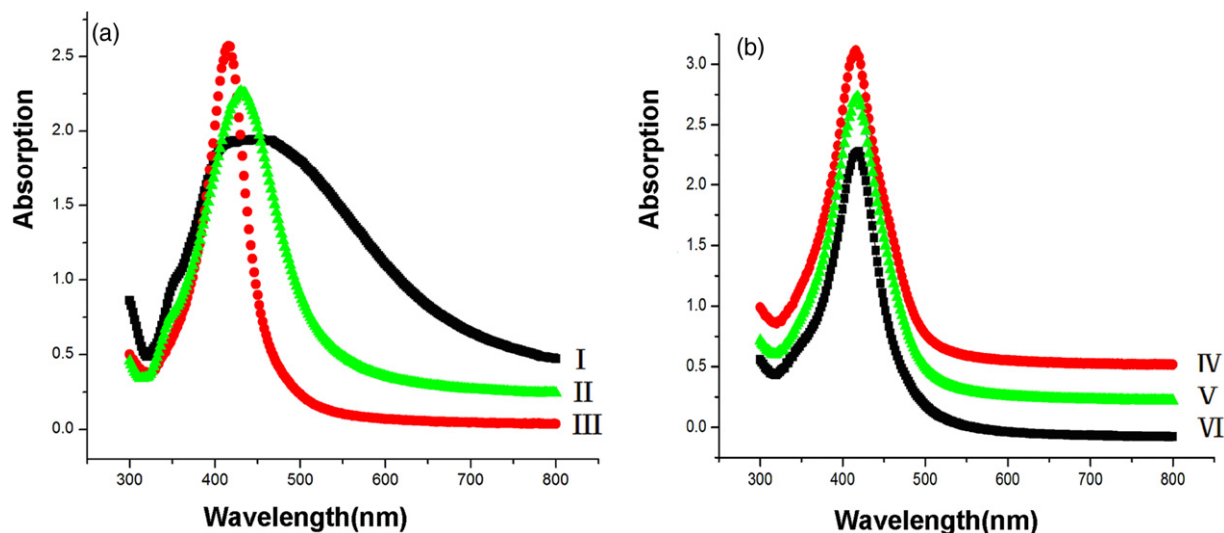


**Figure 1.** UV spectra of the synthesized silver nanoparticles: (a) the reductants were adipic dihydrazide (456 nm, curve I), dextrose (428 nm, curve II) and the mixed reductants (408 nm, curve III) respectively; (b) the PVP/AgNO<sub>3</sub> mass ratios were 3:1 (410 nm, curve IV), 2:1 (412 nm, curve V) and 1:1 (413 nm, curve VI) with the same mixed reductants.

operated at 200 kV. The samples for TEM were prepared by dispersing the final nanoparticles in ethanol and the dispersion was then dropped on carbon-copper grids. The size distribution and number-average nanoparticle diameter were obtained using an Image ProPlus Image Analysis System. The morphology of the silver nanoparticles of the printed electrical patterns before and after sintering was investigated by JSM-6700F scanning electron microscopy (JEOL, Japan). An FV1000-IX81 confocal laser scanning microscope (Olympus, Japan) was also used for investigating the 3d image of the printed lines. The chip bonding process was carried out with the flip-chip technological device Winteen-RFID-PS-2005C (Winteen, China).

### 3. Results and discussion

#### 3.1. UV spectra of the silver nanoparticles

According to Mie's theory [21], the position and shape of the adsorption peaks attributed to the surface plasmon resonance are strongly dependant on the nature of the metal nanoparticles, such as the size, shape, and status of aggregation of the particles [22]. Figure 1(a) shows UV-vis spectra of the silver nanoparticles in aqueous solution when the reductants were adipic dihydrazide (456 nm, curve I), dextrose (428 nm, curve II) and the mixed reductants (408 nm, curve III) respectively. From figure 1(a), the peak shape in curve I was asymmetrical and broad, which suggested that the formed silver nanoparticles reduced by adipic dihydrazide were agminate and had a wide size distribution. The peak shapes in curves II and III were symmetrical, and this showed that the synthesized nanoparticles were not agminated [23]. Moreover, the absorption peak position in curve II shifted toward red wavelengths compared with that in curve III, which indicated that the silver nanoparticles reduced by dextrose were larger than those by mixed reductants. All these results were further demonstrated in figures 2(a)–(c) by TEM images.

Figure 1(b) compares the UV-vis spectra of as-synthesized silver nanoparticles obtained from three different protectant/precursor (PVP/AgNO<sub>3</sub>) mass ratios reduced by mixed reductants. The peak positions for curves IV, V and VI were determined to be at 410, 412 and 413 nm, corresponding to PVP/AgNO<sub>3</sub> mass ratios of 3:1, 2:1 and 1:1 respectively. The half-peak widths of the absorption peaks in figure 1(b) were very narrow, which suggested that the synthesized silver nanoparticles had a narrow size distribution. The change in the peak position was very small on decreasing the PVP/AgNO<sub>3</sub> mass ratio, which proved that this method could synthesize monodisperse silver nanoparticles at low PVP/AgNO<sub>3</sub> mass ratio, and this would greatly reduce the nanofabrication cost and be favorable to ink-jet electrocircuits. The diameter and distribution of the synthesized nanoparticles were further confirmed in figures 2(d)–(f) by TEM analysis of the samples.

#### 3.2. TEM of the silver nanoparticles

In figures 2(a)–(c), TEM micrographs of silver nanoparticles synthesized with adipic dihydrazide, dextrose and the mixed reductants respectively are presented. In theory, the nanoparticle size and distribution from a chemical synthesis process depend upon the relative rates of nucleation and growth processes, as well as the agglomeration [24]. Compared with figures 2(b) and (c), the silver nanoparticles in figure 2(a) are irregular, agminate and larger. This is probably because adipic dihydrazide has a relatively strong reducing power, and overfull crystal nuclei were formed for an instant when it was added into the reaction system. PVP as protectant could not absorb onto the nuclei promptly at this moment, accordingly leading to the aggregation of nuclei into irregular and larger nanoparticles. In contrast, although dextrose had a lower reducing power and nucleation rate, insufficiency of the crystal nuclei caused them to grow into different sized silver nanoparticles as the reaction progressed (figure 2(b)).

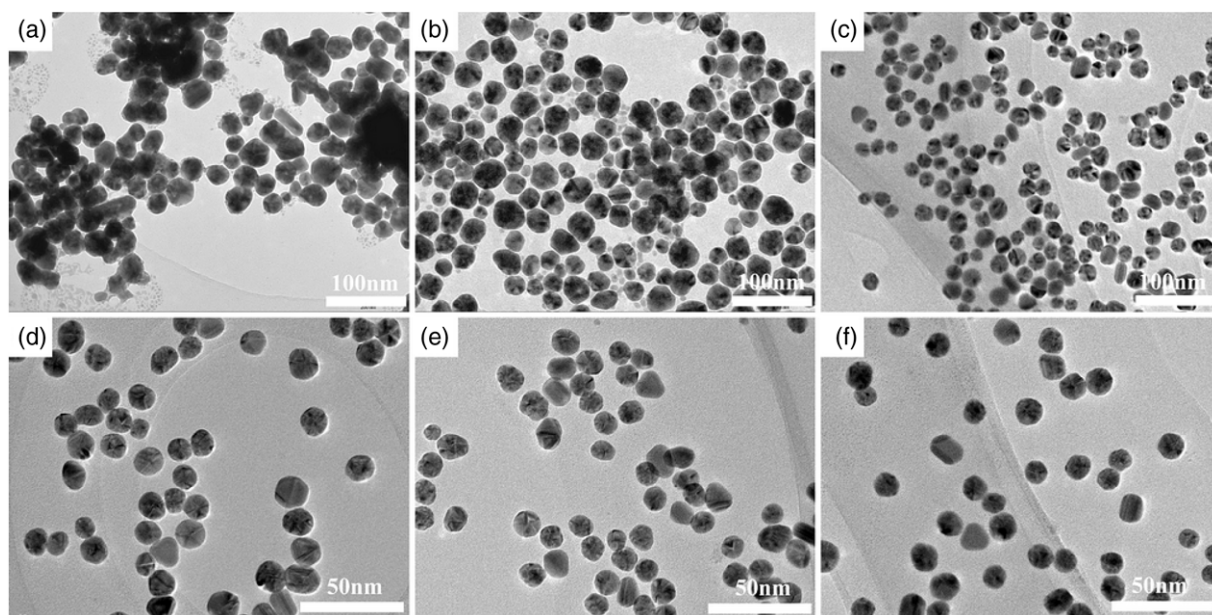


**Figure 2.** TEM of the silver nanoparticles reduced by adipic dihydrazide (a), dextrose (b) and the mixed reductants (c), TEM of the silver nanoparticles synthesized in PVP/AgNO<sub>3</sub> mass ratios of 3:1 (d), 2:1 (e) and 1:1 (f) with the same mixed reductants.

As far as the mixed reductants are concerned, the size and distribution of the synthesized silver nanoparticles could be regulated by controlling the reducing power of the mixed reductants. By regulating the adipic dihydrazide/dextrose ratio, the silver atoms reduced by dihydrazide rapidly formed crystal nuclei at the beginning and maintained an appropriate number, and the later silver atoms reduced by dextrose aggregated on the formed crystal nucleus surfaces and grew into nanoparticles. The formation process of the silver nanoparticles included fast nucleation and a slow growth period, and it was an effective method to prepare monodisperse nanoparticles. The monodisperse silver nanoparticles in figure 2(c) were synthesized with this method.

Furthermore, the effects of the PVP/AgNO<sub>3</sub> mass ratio on the size and distribution of the synthesized silver nanoparticles reduced by mixed reductants were investigated. As shown in figures 2(d)–(f), all the silver nanoparticles were almost spherical and had a narrow distribution. The average size of the synthesized nanoparticles had little difference, i.e.,  $19.1 \pm 1.7$ ,  $21.3 \pm 1.2$  and  $22 \pm 1.8$  nm corresponding to PVP/AgNO<sub>3</sub> mass ratios of 3:1, 2:1 and 1:1 respectively, which was also supported by the plasmon absorption band (figure 1(b)). From the statistical results, it was noteworthy that the standard deviation of the diameter of the nanoparticles was very small, so the silver nanoparticles were monodisperse [25]. As mentioned above, the reduction speed of the silver ions in the nucleation and growth processes could be controlled by regulating the adipic dihydrazide/dextrose ratio. After the nucleation, the silver ions were then reduced by dextrose and absorbed on the formed crystal nucleus at a relatively slow rate. During this period, there was sufficient time for the PVP molecules to adsorb onto the silver nucleus surfaces. This would avoid using excess PVP to enhance the absorbing rate and possibility, and a small amount of PVP could effectively prevent the silver nanoparticles from aggregating.

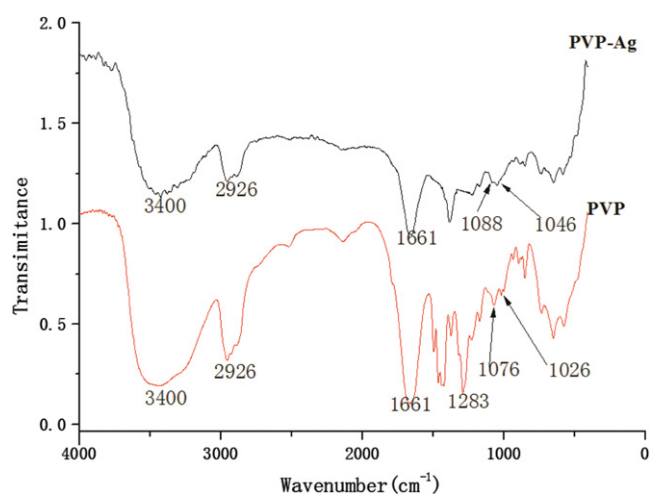


**Figure 3.** IR spectroscopy of the pure PVP and PVP-encapsulated silver nanoparticles.

From the above mentioned results, by this facile and rapid method, monodisperse silver nanoparticles with a size about 20 nm could be synthesized in low PVP/AgNO<sub>3</sub> mass ratio on a large scale under high concentration. Compared with previous reports, the decrease in PVP quantity to prepare monodisperse silver nanoparticles was quite significant, which would reduce the nanofabrication cost and be beneficial to the conductivity of the ink-jet printed flexible electrocircuits.

### 3.3. IR spectroscopy of the silver nanoparticles

The infrared spectra of the PVP-encapsulated silver nanoparticles and pure PVP are shown in figure 3. Compared with the spectra of pure PVP, the characteristic resonance peaks in the spectra of PVP-encapsulated silver nanoparticles around

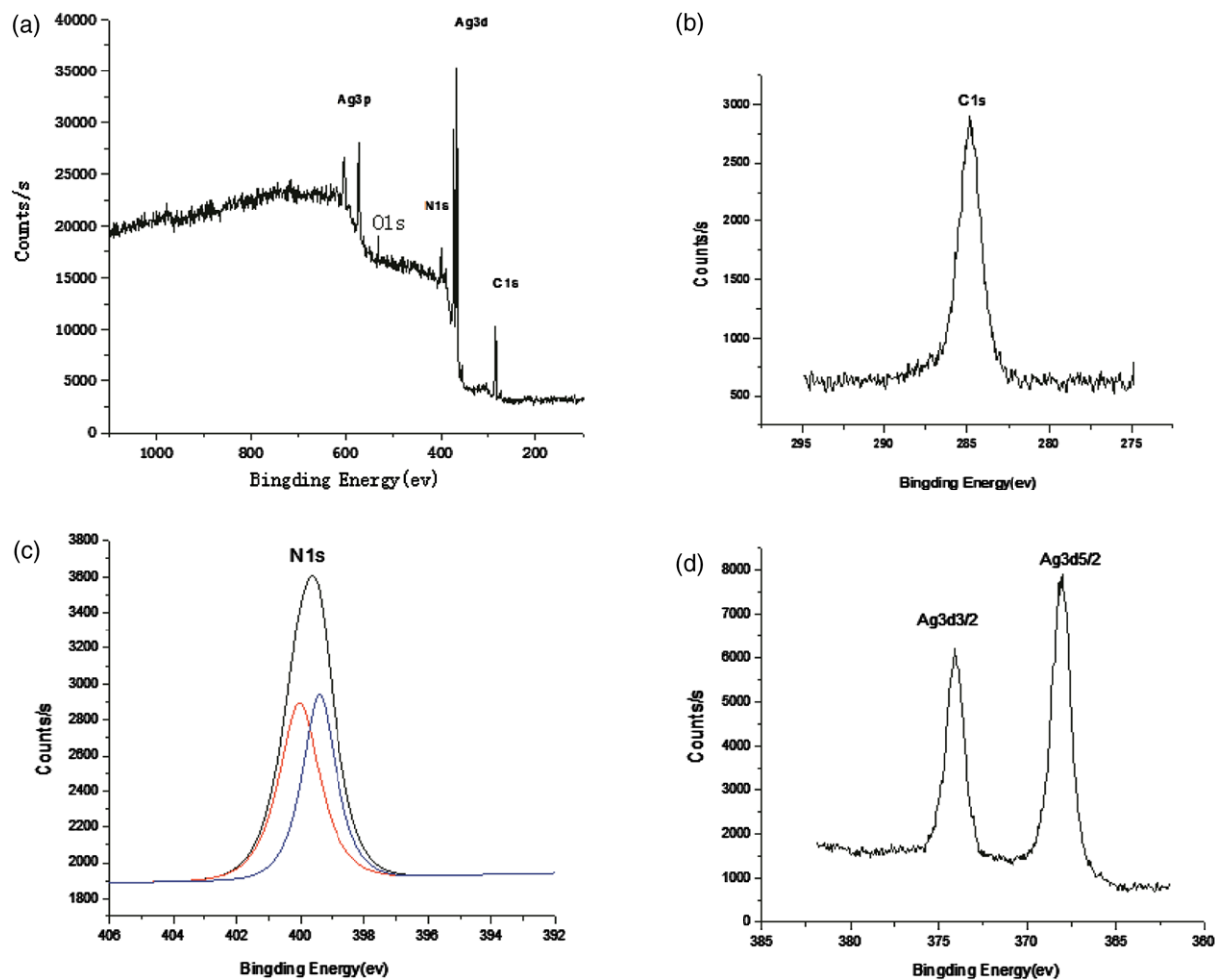


**Figure 4.** XPS spectra of PVP-encapsulated silver nanoparticles: (a) XPS survey spectrum, (b) binding energy spectrum for C 1s, (c) binding energy spectrum for N 1s and (d) binding energy spectrum for Ag 3d.

3400 and 2926  $\text{cm}^{-1}$ , assigned to  $-\text{OH}$  and  $-\text{CH}_2$  stretching vibration respectively, had no changes. For the analysis of which element or group in PVP absorbed to silver and formed the valence bond, the C–N and C=O bonds were selectively chosen. The stretching vibration peak of C=O at 1661  $\text{cm}^{-1}$  has only a small change in size and no change in position; however, the stretching vibration peaks of C–N, originally at 1026 and 1076  $\text{cm}^{-1}$  in pure PVP, were strengthened and red shifted to 1046 and 1088  $\text{cm}^{-1}$  [26]. The changes indicated that the coordination between N atoms and silver nanoparticles was strong, and that between O atoms and silver nanoparticles was relatively weaker. This result further proved that the N atom in PVP molecules was the primary factor to coordinate with silver nanoparticles and form the protection layer [27].

### 3.4. XPS of the silver nanoparticles

To make clear the encapsulation state of the obtained silver nanoparticles, the XPS technique was employed to detect the composition of the silver nanoparticles (figure 4). The binding energy was referenced to the standard C 1s at 287.60 eV. Figure 4(a) shows the XPS survey spectra of

the purified silver nanoparticles; the atoms of C, N, O and Ag were detected, and no other obvious peaks were found, indicating the high purity of the sample. The binding energies at 287.82 eV and 399.66 eV arose from C 1s and N 1s respectively (figures 4(b) and (c)). The N 1s peak was resolved into two peaks at 398.4 and 399.8 eV respectively. The 398.4 eV peak suggested the presence of charged nitrogen atoms, indicating an electrostatic interaction with the silver surface. The peak at 399.8 eV was assigned to C–N units, which suggested the interaction between these N atoms and the silver nanoparticles. From the spectra of Ag 3d (figure 4(d)), the binding energies for Ag 3d<sub>5/2</sub> and Ag 3d<sub>3/2</sub> were found to be 368.12 eV and 373.96 eV respectively, which were compared to the respective core levels of bulk Ag crystals (368 and 374 eV) [28]. Moreover, the narrow width of the peaks suggested that only a single-element silver was present in the system, and provided evidence for the encapsulation of zero valence silver nanoparticles by PVP macromolecules. The results of the XPS spectra revealed that PVP could stabilize the silver nanoparticles from aggregation and provided supporting evidence for the PVP-encapsulated silver nanoparticle structure.

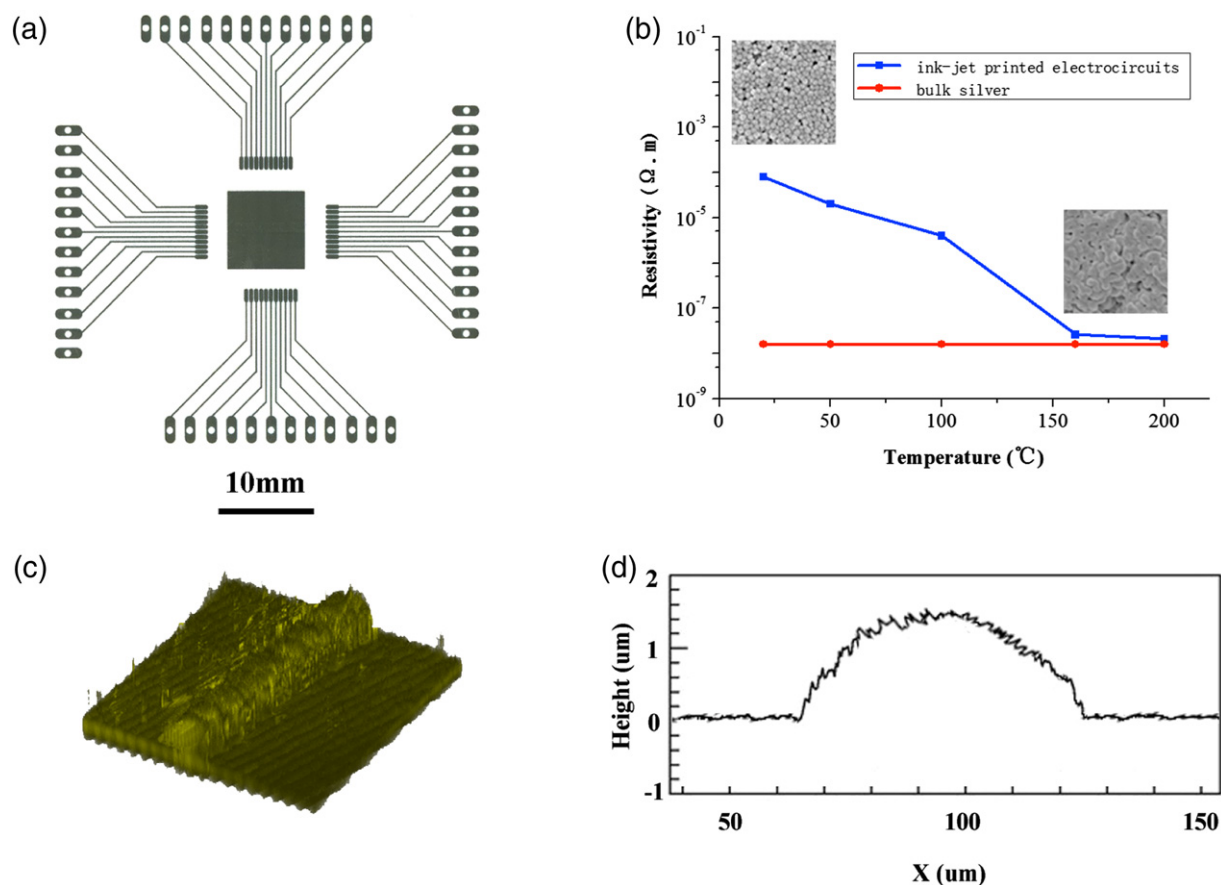


**Figure 5.** The ink-jet printed flexible electrocircuits (a), their resistivities at different sintering temperatures (b), the 3d confocal image (c) and cross-sectional areas (d) of ink-jet printed electrocircuits.

### 3.5. Ink-jet printed flexible electrocircuits

In a typical experiment, a series of flexible electrocircuits as shown in figure 5(a) and figures S1–S3 (in supporting information available at [stacks.iop.org/Nano/22/425601/mmedia](http://stacks.iop.org/Nano/22/425601/mmedia)) were obtained by ink-jet printing silver nanoparticle ink on chrome paper with a commercial Epson C110 printer. This silver layer consisted of a uniform coverage of nanoparticles (figure 5(b), top). The nanoparticles closed together by the convective flow during evaporation of the solvents. However, the residual organic dispersants adsorbed on the surface of the nanoparticles will prevent electrons from moving from one nanoparticle to another [29]. Therefore the resistivity of the ink-jet printed electrocircuits was relatively high due to the scarcity of effectively conducting percolation paths [8].

To achieve lower resistivity, sintering of the nanoparticles was required, and the changes of resistivity at different sintering temperature are shown in figure 5(b). The electrical resistivity,  $\rho$ , was calculated from the resistance  $R$ , the length  $l$ , and the cross-sectional area  $A$  of the line (figure 5(d)), using  $\rho = RA/l$ , and subsequently compared with the value of bulk silver ( $1.586 \times 10^{-8} \Omega \text{ m}$ ). Typically, the ink-jet printed electrocircuits were sintered in a convection oven at  $160^\circ\text{C}$  for 30 min to transform the contact areas to thicker necks and, eventually, to a dense layer (figure 5(b), bottom). In order

to further show the surface topography change of the printed electrocircuits after sintering, they were characterized by SEM and are shown in figure S4 in the supporting information (available at [stacks.iop.org/Nano/22/425601/mmedia](http://stacks.iop.org/Nano/22/425601/mmedia)). From the SEM, the electrocircuits could produce more continuous percolation paths and the conductivity gradually increased as the sintering proceeded [8]. A significantly lower resistivity value was achieved when the sintering temperature was kept at  $160^\circ\text{C}$  for 30 min, and the resistivity decreased in the range of  $9.18 \times 10^{-8}$ – $8.76 \times 10^{-8} \Omega \text{ m}$ , which was five times the bulk silver resistivity. When the sintering temperature was higher than  $160^\circ\text{C}$ , the resistivity in figure 5(b) reached a plateau.

The electrical conductivity of the ink-jet printed electrocircuits was related to their morphology, and depended on the formulation of suitable inks [30]. However, ‘coffee ring’-like structure was commonly obtained after solvent evaporation from the droplet containing most of the solutes [31–33]. This ‘coffee ring’ is undesirable as it could affect the performance of ink-jet printed devices and considerable efforts have been made to eliminate this effect [34]. Several approaches had been proposed to suppress the outward flow and to obtain a flat film, such as control of the initial contact angle of the droplet and the use of a mixed solvent [35]. In this work, the solvent of ethylene glycol, which has a higher boiling point and a lower surface tension than water, can prevent the

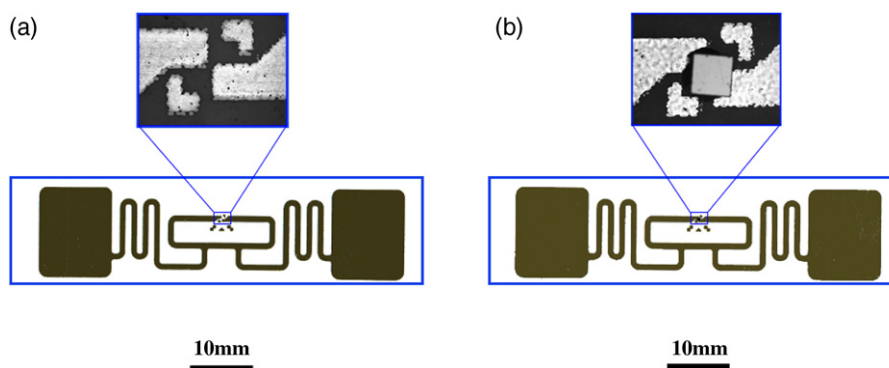


**Figure 6.** (a) The ink-jet printed flexible RFID antenna on paper, chip location close-up view (top), (b) the chip bonded RFID antenna, chip close-up view (top).

outward flow of the solute to the edge of the deposited drop, due to the established Marangoni effect [36]. The 3d confocal microscopy image of the ink-jet printed electrocircuits in figure 5(c) shows relatively uniform surface structure. The nanoparticles were accumulated at the center and the so-called ‘coffee ring effect’ was effectively suppressed.

To further verify the application performance, an RFID antenna electrocircuit according to the Alien-9662 inlay (figure 6(a)) was fabricated by an ink-jetting method. After sintering at 160 °C for 30 min, 6 m signal wireless transmission was achieved after mounting an Alien higgs-3 chip with the flip-chip method (figure 6(b)). Moreover, our conductive ink could be used directly in a commercial printer without any modification of the mechanical system, which made this method low cost and readily applicable for ink-jet printed flexible electrocircuits.

#### 4. Conclusion

In summary, a new reduction system with adipoyl hydrazide and dextrose as mixed reductants was developed to achieve fast nucleus formation and a slow growth process, and monodisperse silver nanoparticles were successfully produced at a low PVP/AgNO<sub>3</sub> mass ratio. In particular, this approach could be conducted on a large scale at high concentration, which was highly beneficial to low cost nanofabrication. The IR and XPS spectra indicated that the N atom in the PVP molecule was the primary factor to coordinate with silver nanoparticles and form the protection layer. A series of flexible electrocircuits were fabricated by ink-jet printing the ink of the as-synthesized silver nanoparticles with a commercial printer. After sintering, the ink-jet printed electrocircuits had low resistivity in the range of  $9.18 \times 10^{-8}$ – $8.76 \times 10^{-8}$  Ω m, which fully met the application in electrocircuits, in particular, in the usage of an RFID antenna. These results promise enormous potential for the manufacture of flexible electrocircuits, low cost electrodes and sensor devices by ink-jet printing.

#### Acknowledgments

This work is supported by the National Nature Science Foundation (Grant Nos 21003132, 21073203, 21004068,

50973117, 51173190, 21074139 and 20904061), and the 973 Program (2007CB936403, 2009CB930404, 2011CB932303 and 2011CB808400).

#### References

- [1] De Gans B J, Hoepfener S and Schubert U S 2006 *Adv. Mater.* **18** 2101
- [2] Kim D, Jeong S, Lee S, Park B K and Moon J 2007 *Thin Solid Films* **515** 7692
- [3] Dearden A L, Smith P J, Shin D Y, Reis N, Derby B and O’Brien P 2005 *Macromol. Rapid Commun.* **26** 315
- [4] Wu Y L, Li Y N and Ong B S 2007 *J. Am. Chem. Soc.* **129** 1862
- [5] Sivaramakrishnan S, Chia P J and Yeo Y C 2007 *Nature Mater.* **6** 149
- [6] Chung J, Ko S, Bieri N R, Grigoropoulos C P and Poulikakos D 2004 *Appl. Phys. Lett.* **84** 801
- [7] Park J and Moon J 2006 *Langmuir* **22** 3506
- [8] Magdassi S, Grouchko M, Tokor D, Kamysnyh A and Balberg I 2005 *Langmuir* **21** 10264
- [9] Kim J, Kim D, Veriansyah B, Kang J W and Kim J D 2009 *Mater. Lett.* **63** 1880
- [10] Huang H H, Yan F Q, Kek Y M, Chew C H, Xu G Q, Ji W, Oh P S and Tang S H 1997 *Langmuir* **13** 172
- [11] Dhas N A, Raj C P and Gedanken A 1998 *Chem. Mater.* **10** 1446
- [12] Harpeness R and Gedanken A 2004 *Langmuir* **20** 3431
- [13] Henglein A 2000 *J. Phys. Chem. B* **104** 1206
- [14] Song X Y, Sun S X, Zhang W M and Yin Z L 2004 *J. Colloid Interface Sci.* **273** 463
- [15] Kim D, Jeong S and Moon J 2006 *Nanotechnology* **16** 4019
- [16] Zhang X Y, Hicks E M, Zhao J, Schatz G C and Duyn R P V 2005 *Nano Lett.* **5** 1503
- [17] He R, Qian X, Yin J and Zhu Z 2002 *J. Mater. Chem.* **12** 3783
- [18] Sun Y and Xia Y N 2002 *Science* **298** 2176
- [19] Silvert P Y, Urbina R H, Duvauchelle N, Vijayakrishnan V and Elhissien K T 1996 *J. Mater. Chem.* **6** 573
- [20] Jolke P, Chris E H, Antonius W M D L and Ulrich S S 2009 *Nanotechnology* **16** 165303
- [21] Mie G 1908 *Ann. Phys.* **25** 377
- [22] Schofield C L, Haines A H, Field R A and Russel D A 2006 *Langmuir* **22** 6707
- [23] Wang D S, Kerker M and Chew H 1980 *Appl. Opt.* **19** 2135
- [24] Zheng N, Fan J and Stucky G D 2007 *J. Am. Chem. Soc.* **128** 6550
- [25] Lin X Z, Teng X and Yang H 2003 *Langmuir* **19** 10081
- [26] Wang H, Qiao X, Chen J, Wang X and Ding S 2005 *Mater. Chem. Phys.* **94** 449

- [27] Zhang Z, Zhao B and Hu L 1996 *J. Solid State Chem.* **121** 105
- [28] Sharma J, Chaki N K, Mandale A B, Pasricha R and Vijayamohan K 2004 *J. Colloid Interface Sci.* **272** 145
- [29] Van Osch T H J, Perelaer J, de Laat A W M and Schubert U S 2008 *Adv. Mater.* **20** 343
- [30] Kim D, Jeong S, Park B K and Moon J 2006 *Appl. Phys. Lett.* **89** 264101
- [31] Shen X, Ho C M and Wong T S 2010 *J. Phys. Chem. B* **114** 5269
- [32] Lee D J and Oh J H 2010 *Surf. Interface Anal.* **42** 1261
- [33] Soltman D, Smith B, Kang H, Morris S J S and Subramanian V 2010 *Langmuir* **26** 15686
- [34] Chow E, Herrmann J, Barton C S, Raguse B and Wieczorek L 2009 *Anal. Chim. Acta* **632** 135
- [35] Kajiya T, Kobayashi W, Okuzono T and Doi M 2009 *J. Phys. Chem. B* **113** 15460
- [36] Park B K, Kim D, Jeong S, Moon J and Kim J S 2007 *Thin Solid Films* **515** 7706